Title
Correction of Artifacts Induced by B_0 Inhomogeneities in Breast MRI Using Reduced-Field-of-View Echo-Planar Imaging and Enhanced Reversed Polarity Gradient Method

Author
Rodriguez-Soto, Ana

Publication Date
2021-05-01

Peer reviewed

ORIGINAL RESEARCH

Correction of Artifacts Induced by B_0 Inhomogeneities in Breast MRI Using Reduced-Field-of-View Echo-Planar Imaging and Enhanced Reversed Polarity Gradient Method

Ana E. Rodríguez-Soto, PhD,[1] Lauren K. Fang, BS,[1] Dominic Holland, PhD,[1] Jingjing Zou, PhD,[2] Helen H. Park, BS,[3] Kathryn E. Keenan, PhD,[4] Hauke Bartsch, PhD,[1] Joshua Kuperman, PhD,[1] Anne M. Wallace, MD,[5] Michael Hahn, MD, PhD,[1] Haydee Ojeda-Fournier, MD,[1] Anders M. Dale, PhD,[1] and Rebecca Rakow-Penner, MD, PhD[1]*

Background: Diffusion-weighted (DW) echo-planar imaging (EPI) is prone to geometric distortions due to B_0 inhomogeneities. Both prospective and retrospective approaches have been developed to decrease and correct such distortions.
Purpose: The purpose of this work was to evaluate the performance of reduced-field-of-view (FOV) acquisition and retrospective distortion correction methods in decreasing distortion artifacts for breast imaging. Coverage of the axilla in reduced-FOV DW magnetic resonance imaging (MRI) and residual distortion were also assessed.
Study Type: Retrospective.
Population/Phantom: Breast phantom and 169 women (52.4 $\pm$ 13.4 years old) undergoing clinical breast MRI.
Field Strength/Sequence: A 3.0 T/ full- and reduced-FOV DW gradient-echo EPI sequence.
Assessment: Performance of reversed polarity gradient (RPG) and FSL topup in correcting breast full- and reduced-FOV EPI data was evaluated using the mutual information (MI) metric between EPI and anatomical images. Two independent breast radiologists determined if coverage on both EPI data sets was adequate to evaluate axillary nodes and identified residual nipple distortion artifacts.
Statistical Tests: Two-way repeated-measures analyses of variance and post hoc tests were used to identify differences between EPI modality and distortion correction method. Generalized linear mixed effects models were used to evaluate differences in axillary coverage and residual nipple distortion.
Results: In a breast phantom, residual distortions were 0.16 $\pm$ 0.07 cm and 0.22 $\pm$ 0.13 cm in reduced- and full-FOV EPI with both methods, respectively. In patients, MI significantly increased after distortion correction of full-FOV (11 $\pm$ 5% and 18 $\pm$ 9%, RPG and topup) and reduced-FOV (8 $\pm$ 4% both) EPI data. Axillary nodes were observed in 99% and 69% of the cases in full- and reduced-FOV EPI images. Residual distortion was observed in 93% and 0% of the cases in full- and reduced-FOV images.
Data Conclusion: Minimal distortion was achieved with RPG applied to reduced-FOV EPI data. RPG improved distortions for full-FOV images but with more modest improvements and limited correction near the nipple.
Evidence Level: 3
Technical Efficacy: Stage 1

J. MAGN. RESON. IMAGING 2021;53:1581–1591.

View this article online at wileyonlinelibrary.com. DOI: 10.1002/jmri.27566

Received Jul 20, 2020, Accepted for publication Feb 3, 2021.

*Address reprint requests to: R.R.-P., 9400 Campus Point Drive #7316, La Jolla, CA 92093, USA. E-mail: rrakowpenner@ucsd.edu
Certain commercial instruments and software are identified to specify the experimental study adequately. This does not imply endorsement by National Institute of Standards and Technology (NIST) or that the instruments and software are the best available for the purpose.

From the [1]Department of Radiology, University of California, San Diego, La Jolla, California, USA; [2]Division of Biostatistics and Bioinformatics, Herbert Wertheim School of Public Health and Human Longevity Science, University of California, San Diego, La Jolla, California, USA; [3]School of Medicine, University of California, San Diego, La Jolla, California, USA; [4]National Institute of Standards and Technology Boulder, Colorado, USA; and [5]Department of Surgery, University of California, San Diego, La Jolla, California, USA

Breast cancer is the most common cancer in American women after skin cancer.[1] It is estimated that one in eight U.S. women will develop a form of breast cancer in their lifetime, emphasizing the importance of effective and accurate screening practices.[2] Breast magnetic resonance imaging (MRI) is currently used for screening women with high-risk breast cancer[3], evaluating new breast cancer diagnosis,[4] and other indications such as response to neoadjuvant chemotherapy.[5] Clinical breast MRI protocols include contrast-enhanced (CE)-MRI in which intravenous contrast agents are administered to visualize vascular patterns, such as tumor angiogenesis.[6] As a result, CE-MRI has high sensitivity but moderate specificity for breast cancer detection.[6]

Brain and bone depositions of such contrast agents have been reported in patients with cumulative exposure with unknown sequelae.[7] Hence, there is a need for the development of contrast-free MRI protocols and thus reduce the number of patients who undergo contrast exposure. Diffusion-weighted (DW) MRI has been incorporated into breast MRI protocols and has been proposed as a contrast-free screening tool for breast cancer.[8] While the combined use of CE- and DW-MRI improves cancer detection sensitivity and specificity compared to either technique individually,[6] the value of DW-MRI as a stand-alone noncontrast screening technique remains to be demonstrated. Its current utility in breast imaging is mostly to evaluate response to treatment in patients with known malignancy.[9] Its widespread clinical use has been severely hampered by distortion artifacts and limited spatial resolution, which limit the accurate location of lesions.

DW-MRI is commonly acquired using a single-shot echo-planar imaging (EPI) readout, which minimizes acquisition time by continuously traversing k-space. However, spatial and intensity distortions occur in regions of B_0 inhomogeneities, which arise at air-tissue interfaces (eg, anterior chest wall and breast tissue boundaries) due to magnetic susceptibility differences. In EPI, the bandwidth in the phase encoding (PE) direction is much lower than that in the frequency encoding direction. Because of the low bandwidth in the PE direction (equivalently, because of the relatively long time between sampling points in that direction), these artifacts predominantly appear in the PE direction.[10] Geometrically distorted DW-MRI limits the accurate location of tumor lesions. In breast imaging, these artifacts are pronounced due to off-isocenter scanning and the complexity of the anatomy.

Efforts to decrease geometric distortions present in DW-EPI for breast imaging include both acquisition and postprocessing distortion-correcting methods.[11] In general, acquisition strategies decrease the lines collected in the PE direction, which reduces the readout duration and shortens the time during which spin dephasing due to B_0 inhomogeneities evolves. These strategies include parallel imaging, multishot imaging (in either the frequency or PE directions),[11] and reduced-field-of-view (FOV) imaging.[12] In the latter, spins are excited within a reduced FOV in the PE direction, resulting in a rectangular FOV.[12] The use of reduced FOV in DW-EPI was shown to increase in-plane resolution and reduce geometric distortions, initially in the spinal cord,[12] and subsequently in other organs such as prostate,[13] pancreas,[14] kidneys[15], and breast.[16]

Postprocessing distortion correction algorithms most commonly rely on field mapping to estimate local off-resonance across images.[16] In contrast, Holland et al developed a distortion correction method that exploits the symmetry of the artifacts in the positive and negative PE trajectories[17]: regions with spins that become compressed in images collected with a given PE trajectory polarity (eg, anterior–posterior, A/P) will be expanded in images collected with the opposite trajectory polarity (eg, posterior–anterior, P/A). This approach, termed reversed polarity gradient (RPG), requires the acquisition of two non-DW, b = 0 s/mm^2 or low b-value volumes, one with positive and one with negative PE direction. When using a pulse sequence in which single-shot positive and negative PE directions are collected one after the other, the cost in acquisition time is an additional repetition time (TR). These data are used to estimate the deformation field that minimizes the difference between both volumes and to unwarp the DW volumes. Previous studies have shown that the use of RPG improved the localization of brain, prostate, and breast tumor lesions.[17–19]

Reduced-FOV EPI produces images with fewer geometric distortions, but it does not eliminate them. Given the importance of accurate cancer localization in breast cancer screening and monitoring practices, investigating the application of reduced-FOV EPI and RPG in breast MRI is necessary. Therefore, the purpose of this study was to evaluate the sole and combined performance of these acquisition and postprocessing distortion-correction strategies for breast MRI.

Methods

Phantom Studies

A breast phantom designed by the University of California San Francisco and the National Institute of Standards and Technology[20] was scanned using a 3-T MRI scanner (MR750; GE Healthcare, Milwaukee, Wisconsin, USA) and a breast array coil. Low b-value volumes of DW-EPI and rapid acquisition with relaxation enhancement (RARE) images were acquired. Pulse sequence parameters: 1) *fat suppressed RARE*: TE/TR = 107/4520 msec, refocusing pulse flip angle of 111°, FOV = 320×320 mm^2, acquisition matrix 512×320, reconstruction matrix 512×512, interpolated voxel size = $0.625 \times 0.625 \times 5$ mm^3; 2) *full-FOV DW-MRI*: TE/TR = 82/9000 msec, b-values (number of diffusion directions) = 0, 500 (6), 1500 (6), and 4000 (15) s/mm^2, FOV = 320×320 mm^2, acquisition matrix 96×96, interpolated voxel size = $2.5 \times 2.5 \times 5$ mm^3, scan duration 4.5 minutes, spectral attenuated inversion recovery (SPAIR) fat suppression, PE direction left–right (L/R), no parallel imaging; and 3) *reduced-FOV DW-MRI*: TE/TR = 82/9000 msec, FOV = 160×320 mm^2, acquisition matrix 48×96, reconstruction matrix 128×128, interpolated voxel size = $2.5 \times 2.5 \times 5$ mm^3, scan duration 4.5 minutes, SPAIR fat suppression, PE direction A/P, no parallel imaging. Negative PE direction was only collected for low b-value volumes. Pulse sequence parameters between full- and reduced-FOV DW-MRI data were identical except for the PE direction and the FOV in the PE direction. Because TR and the number of slices were identical between DW-MRI pulse sequences, scan time durations were the same.

The breast phantom contains a polycarbonate plate with a grid of circles spaced at 1.5-cm intervals. The spatial discrepancy in the center of each circle between EPI and RARE images was measured to quantify the magnitude of the initial distortion and to evaluate the performance of RPG. The phantom also contains tubes with different concentration of polyvinylpyrrolidone (PVP) to change the apparent diffusion coefficient (ADC) of the phantom contents. The ADC maps of each FOV data set were generated before and after distortion correction with RPG and topup. Regions of interest (ROIs) surrounding the tubes inside the breast phantom (four tubes with 10% PVP, one tube with 14% PVP, one tube with 18% PVP, two tubes with 25% PVP, three tubes with 40% PVP, and one tube with H_2O) were manually drawn on the most central slice using Osirix (Pixmeo, Geneva, Switzerland). These ROIs were used to extract ADC values. Average, standard deviation, and coefficient of variation (CV) for each PVP concentration (and water) are reported.

In Vivo Studies

A waiver of consent was granted by the Institutional Review Board to perform this retrospective study of breast MRI examinations. The MRI data in the present study were acquired using the institution's standard of care clinical imaging protocol.

In this retrospective study, diagnostic and surveillance MRI was performed in 169 women (52.4 ± 13.4 years old) between January 2016 and July 2019, as part of the standard-of-care MRI protocol at our institution. Patients were scanned in the prone position using identical setup and pulse sequence parameters as described above (except in some cases, FOV was 360×360 mm^2 or 180×360 mm^2 with the same acquisition matrix and increased voxel size). Full-FOV DW-MRI was acquired with PE in the L/R direction to minimize cardiac motion artifacts. However, due to the rectangular geometry of the reduced FOV, these images were acquired with PE in the A/P direction. Of note, both PE trajectory polarities were collected sequentially to minimize differences between the volumes that were unrelated to the change in PE polarity (eg, subject motion, vessel pulsatility).

Distortion Correction Algorithm

Both full- and reduced-FOV EPI volumes were collected in the positive and negative PE trajectories to retrospectively correct for B_0-inhomogeneity-induced artifacts with RPG. Input volumes (positive and negative PE trajectories) were resampled to a resolution of $2 \times 2 \times 2$ mm^3. Briefly, the distortion correction algorithm was as follows: 1) positive and negative images were blurred with a Gaussian kernel of determined width (the initial kernel size was user-defined); 2) blurred positive and negative images were registered to each other, i.e. the displacement field was calculated by minimizing the cost function *f*, defined below, as described by Holland et al; 3) the displacement field that aligned both images was used to inform and update the deformation field that corrected original positive and negative volumes; and 4) the width of the Gaussian kernel used in step 1 was reduced. Steps 1–4 were repeated until the kernel width was zero. With an incrementally improving displacement field, updated corrected images were built from the original images using a single cumulative deformation field.[17] The cost function *f* was defined as

$$f(u_1,\ldots,u_N) = \frac{1}{N}\sum_{i=1}^{N}\left[J_{1i}I_1\left(\vec{r}_i + u_i\hat{y}\right) - J_{2i}I_2\left(\vec{r}_i - u_i\hat{y}\right)\right]^2 + \lambda_1\sum_{i=1}^{N}u_i^2 + \lambda_2\sum_{i=1}^{N}\left[\vec{\nabla}_i u_i\right]^2$$

where u_i is the displacement shift of the *i*th voxel located at $\vec{r}_i = (x_i, y_i, z_i)$ that corrects the distorted images in the positive and negative PE trajectories I_1 and I_2, respectively; J_1 and J_2 are the Jacobian of the transformation between uncorrected and distortion corrected images; and λ_1 and λ_2 are the regularization parameters of the model that control the variability of the three-dimensional displacement field. Displacement fields estimated from isotropic volumes were then properly scaled to the original voxel size and applied to the positive and negative PE direction volumes. In addition, the originally implemented proton density correction (normalization by the Jacobian of the resulting displacement field) was removed. This last processing step was removed as, in the author's experience, it introduced an artificial appearance of improved distortion together with spurious signals when small discrepancies (i.e. respiration or pulsatility motion) exist between positive and negative PE trajectories.

Each EPI data set was distortion-corrected with RPG using all combinations of Gaussian kernel width (60, 70, and 80 pixels) and λ_2 (500, 1500, and 2500 arbitrary units [a.u.], with smaller values allowing for a more varying deformation field) to account for B_0-inhomogeneity variation across

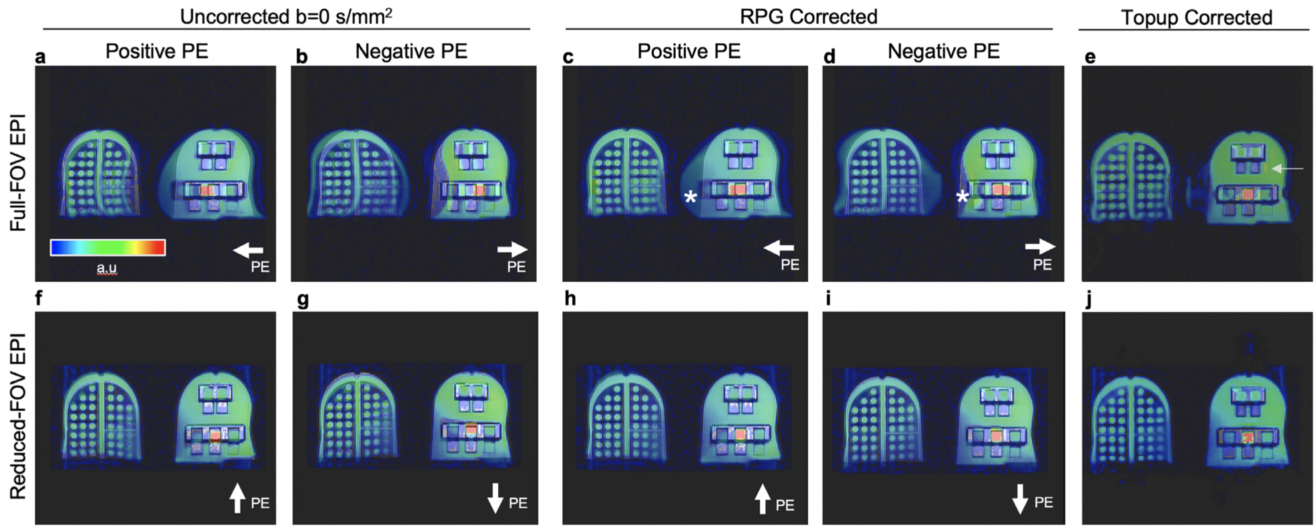

FIGURE 1: Overlay of positive and negative PE trajectory polarities of both full-FOV (a,b) and reduced-FOV (f,g) EPI on RARE images of a breast phantom. Note that the full- and reduced-FOV images have different PE directions. The solution in the phantom interstitial space (shades of green) is fibroglandular tissue mimic consisting of 35% corn syrup in deionized water. The high-signal region (red in overlay) is 25% PVP used to mimic tumor diffusion properties and the low-signal regions (blue) are fat mimic (grape seed oil). Full- and reduced-FOV EPI data were distortion corrected using the RPG (c,d,h,i) and FSL topup (e,j) methods. The RPG algorithm performs well when unwarping regions within the breast phantom structures as observed in the distortion plate (grid of circles spaced at constant intervals). However, distortion correction is limited on the medial region of the phantom (asterisks) in full-FOV EPI. Topup performs well in the medial region but introduces signal intensity artifacts (white arrow) in full-FOV images. Outputs of RPG and topup have similar, but not identical, signal intensity ranges. a.u. = arbitrary units; PE = phase encoding; EPI = echo-planar imaging; FOV = field of view; RPG = reversed polarity gradient; PVP = polyvinylpyrrolidone; RARE = rapid acquisition with relaxation enhancement.

subjects. The distortion-corrected data set with the highest mutual information (MI)[21] between corrected positive and negative PE trajectory volumes was determined to be the most correct for each subject.

In addition, FMRIB's software library (FSL, v5.0, Oxford, UK) topup distortion correction[22] was performed on both phantom and in vivo data to compare to the performance of RPG. The FSL-supplied configuration file containing combinations of optimization parameters was modified to evaluate values of full width at half maximum of Gaussian smoothing ranging from 1 to 10 mm. Similar to the selection of RPG parameters, the distortion-corrected data set with the highest MI between the corrected positive and negative PE trajectory volumes was selected for each subject. There are many similarities between the RPG approach and topup as they both rely on the positive and negative PE trajectories for distortion correction. One major difference in implementation, however, is that topup continues to perform proton density correction (normalization by the Jacobian of the resulting displacement field).

In order to evaluate the performance of the distortion correction algorithm, MI was estimated between RARE images and the positive PE volume before and after distortion correction with both RPG and FSL's topup. The average, median, mode, and 95th percentile absolute deformation between original and distortion corrected low b-value volumes were computed. Results were reported within the constrained FOV for both the full- and reduced-FOV data sets.

The RARE and DW images after distortion correction with RPG were read by two independent breast radiologists (R.R.P and H.O.F.) to evaluate if coverage on reduced-FOV DW-MRI is adequate to evaluate axillary nodes compared to full-FOV DW images and identify residual distortion artifacts in the nipple area between full- and reduced-FOV DW-MRI. Readers were asked the following questions: 1) Can axillary nodes be evaluated? Answers to the question were Yes, No, and Partially; 2) Is there residual distortion in the nipple region? Answers to this question were either Yes or No.

Statistical Tests

All statistical analyses were performed using SPSS statistics software (version 26 for Mac OS X; IBM Corporation, Armonk, NY, USA). The threshold for significance (α) was set at 0.05 for all analyses. Differences in MI, displacements, and ADC values were compared using two-way repeated-measures analyses of variance with Sidak post hoc tests to identify significant differences between EPI modality (full and reduced FOV) and distortion correction method (RPG and topup). All data are reported as mean $\pm$ standard deviation values. Generalized linear mixed effects models with a logit link function and binomial probability distribution were used to evaluate differences in axillary coverage and residual nipple distortion between full- and reduced-FOV DW-MRI. For statistical analysis, cases with partial axillary coverage were considered as having no axillary coverage. The differences in axillary coverage and residual nipple distortion were evaluated

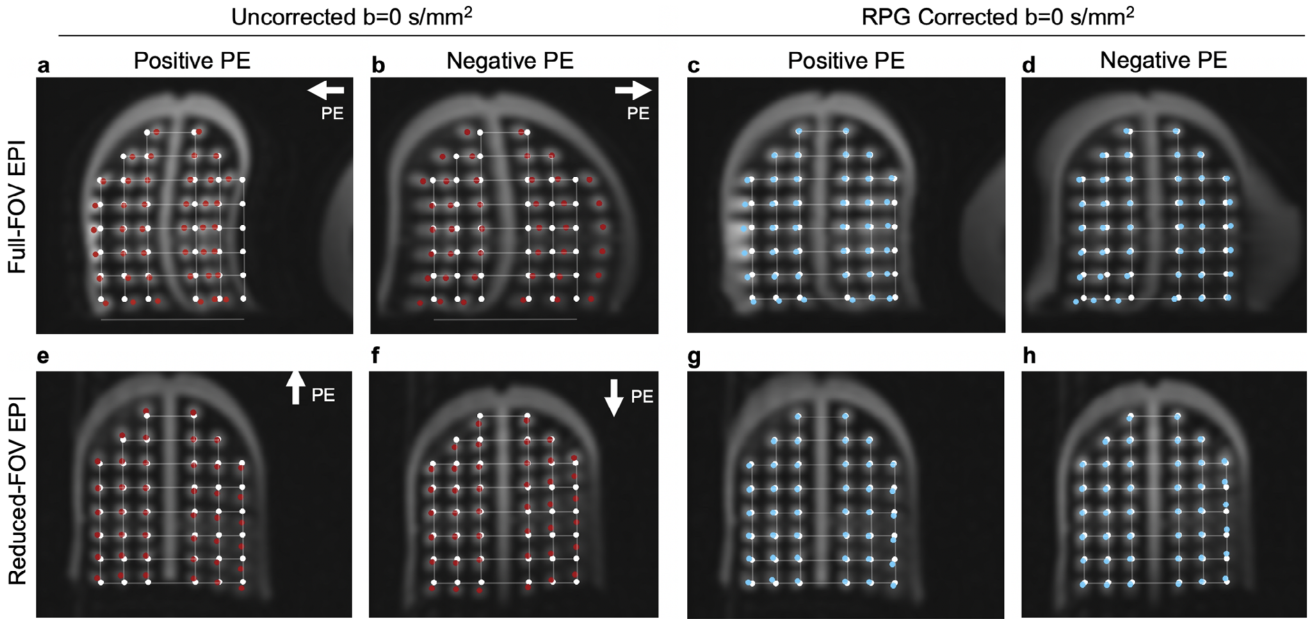

FIGURE 2: Full-FOV (a–d) and reduced-FOV EPI (e–h) before (a, b, e and f) and after (c, d, g and h) distortion correction with the RPG method in a breast phantom. White points indicate the location of the center of each circle on the polycarbonate grid on the RARE image. Red and blue points indicate the center (maximum signal intensity) of each circle on full- and reduced-FOV EPI data before and after distortion correction, respectively. Full- and reduced-FOV images have different PE directions. PE = phase encoding; EPI = echo-planar imaging; FOV = field of view; RPG = reversed polarity gradient; RARE = rapid acquisition with relaxation enhancement.

via the effects of the imaging method indicator (full- or reduced-FOV) on the outcomes of readers' responses while adjusting for within-subject correlations using random effects and reader indicator using fixed effects. In addition, inter-reader agreements were evaluated using exact McNemar's test and Cohen's Kappa stratified by outcomes (axillary coverage and residual nipple distortion) and EPI modality (full- or reduced-FOV DW-MRI).

Results

Uncorrected and distortion-corrected images and the estimated displacement field for breast phantom data are shown in Figure 1. The initial and residual distortion was estimated using the grid of circles within the phantom on EPI and RARE images (Figure 2 and Table 1). Initial distortion was significantly ($P < 0.05$) decreased by a factor of two on reduced-FOV EPI (0.27 ± 0.18 cm) compared to full-FOV EPI (0.54 ± 0.46 cm). After correction with both RPG and topup, the residual distortion was 0.35 times smaller ($P < 0.05$) in reduced-FOV (0.15 ± 0.07 and 0.16 ± 0.08 cm, respectively) than in full-FOV EPI (0.23 ± 0.14 and 0.22 ± 0.12 cm, respectively). No difference was found between residual distortions post-distortion correction with either method. Both RPG and topup improved distortions within the breast phantom structure for both full- and reduced-FOV EPI. However, both techniques have limitations. The performance of RPG was limited in full-FOV EPI near the edges of both sides of the breast phantom (asterisks in Figure 1). Average and 95th percentile displacement postdistortion correction for full-FOV EPI data were significantly ($P < 0.05$) larger (0.2 ± 0.3 cm and 0.7 cm) than that for reduced-FOV EPI data (0.1 ± 0.1 cm and 0.3 cm). The performance of topup is limited by incorporated spurious signal intensity variations in homogeneous regions of the breast phantom (Figure 1).

No differences were detected in ADC values before and after distortion correction with either method (Table 2). However, a significant ($P < 0.05$) reduction in CV post-distortion correction with both RPG and topup methods was identified in full-FOV EPI data. No improvements in CV were detected in reduced-FOV images after distortion correction with either method.

Demographic and disease data of patients included in this study are shown in Table 3. Representative in vivo cases are shown in Figure 3 for women with different breast shapes. There was a significant ($P < 0.05$) increase in MI between full-FOV EPI data and RARE images after distortion correction with RPG and topup of $11\% \pm 5\%$ and $18\% \pm 9\%$, respectively. Furthermore, the increment in MI was higher ($P < 0.05$) for topup compared to RPG. Similarly, MI was increased by $8\% \pm 4\%$ ($P < 0.05$) in reduced-FOV EPI data after correction with both RPG and topup. Overall, the MI between full-FOV EPI and RARE images was higher ($P < 0.05$) than that between reduced-FOV EPI and RARE images. The modes of the displacement fields between uncorrected and corrected full-FOV EPI images were 0.3 ± 0.3 cm and 0.4 ± 0.3 cm when corrected with RPG and topup, respectively. While the modes of displacement for

TABLE 1. Average (±SD) Distance Between Circle Centers on the Polycarbonate Grid of the Breast Phantom Between Echo-Planar Imaging (EPI) and Rapid Acquisition With Relaxation Enhancement (RARE) Images, Before and After Distortion Correction With Reversed Polarity Gradient (RPG) and Topup

	Full-FOV EPI Positive PE (cm)	Full-FOV EPI Negative PE (cm)	Reduced-FOV EPI Positive PE (cm)	Reduced-FOV EPI Negative PE (cm)
Uncorrected	0.54 ± 0.46 (0.01–1.79)	0.59 ± 0.44 (0.02–1.71)	0.27 ± 0.18 (0.04–0.74)	0.31 ± 0.19 (0.04–0.80)
After RPG	0.23 ± 0.14 (0.04–0.52)	0.21 ± 0.19 (0.02–0.89)	0.15 ± 0.07 (0.04–0.35)	0.15 ± 0.08 (0.05–0.43)
After topup	0.22 ± 0.12 (0.02–0.52)	0.21 ± 0.18 (0.01–0.88)	0.16 ± 0.08 (0.06–0.40)	0.15 ± 0.09 (0.04–0.42)

Values in parenthesis indicate range of values.

TABLE 2. ADCs of the Breast Phantom Before and After Distortion Correction Artifacts With Both RPG and Topup

FOV	ADC From Full-FOV Images ($\times 10^{-3}$ mm^2/s)			ADC From Reduced-FOV Images ($\times 10^{-3}$ mm^2/s)		
Phantom Element Concentration	Before Correction	After RPG	After Topup	Before Correction	After RPG	After Topup
10% PVP	1.2 ± 0.3 (29.1%)	1.3 ± 0.2 (17.4%)	1.2 ± 0.3 (27.8%)	1.1 ± 0.3 (27.0%)	1.1 ± 0.3 (25.9%)	1.1 ± 0.3 (24.8%)
14% PVP	1.2 ± 0.3 (23.1%)	1.2 ± 0.3 (20.4%)	1.2 ± 0.2 (19.0%)	1.1 ± 0.3 (32.4%)	1.1 ± 0.3 (25.8%)	1.2 ± 0.4 (21.3%)
18% PVP	1.2 ± 0.2 (20.1%)	1.2 ± 0.2 (16.3%)	1.2 ± 0.2 (14.7%)	1.1 ± 0.2 (21.5%)	1.1 ± 0.2 (22.6%)	1.2 ± 0.2 (16.3%)
25% PVP	1.0 ± 0.2 (20.2%)	1.0 ± 0.2 (15.3%)	1.0 ± 0.2 (18.8%)	1.0 ± 0.2 (17.1%)	1.0 ± 0.2 (16.2%)	1.0 ± 0.2 (16.8%)
40% PVP	0.6 ± 0.2 (25.0%)	0.7 ± 0.1 (20.6%)	0.6 ± 0.1 (22.3%)	0.7 ± 0.2 (35.0%)	0.7 ± 0.2 (35.3%)	0.7 ± 0.2 (32.2%)
H_2O	1.2 ± 0.3 (27.4%)	1.4 ± 0.2 (18.0%)	1.3 ± 0.3 (19.8%)	1.0 ± 0.3 (31.0%)	1.1 ± 0.3 (28.7%)	1.1 ± 0.3 (27.7%)

Results are reported as average and standard deviation. Values in parenthesis represent the CV.
ADC = apparent diffusion coefficient; CV = coefficient of variation; CV = coefficient of variation; FOV = field of view; RPG = reversed polarity gradient; PVP = polyvinylpyrrolidone.

TABLE 3. Demographic and Disease Information of Patients

Total number of patients	**169**
Age (years old (±standard deviation)	53 ± 14
Reason for MRI scan	*N* (%)
High-risk screening	38 (22%)
Treatment planning/evaluation	131 (78%)
Total number of breast lesions	231
Malignant	169
DCIS	14
IDC	84
IDC + DCIS/ILC	29
IDC w/lobular or mucinous features	5
ILC	6
Invasive mammary carcinoma	28
Invasive pleomorphic lobular carcinoma	1
Metaplastic carcinoma	2
Benign	62
Without pathology	7
With pathology	55
Atypical ductal hyperplasia	2
Benign mammary tissue	36
Fibroadenoma	11
Focal atypical ductal hyperplasia	2
Intraductal papilloma	2
LCIS	2

DCIS = ductal carcinoma in situ; IDC = invasive ductal carcinoma; ILC = invasive lobular carcinoma; LCIS = lobular carcinoma in situ; MRI = magnetic resonance imaging.

reduced-FOV data sets were 0.1 ± 0.1 cm and 0.1 ± 0.2 cm, the 95th percentiles were 1.2 ± 0.3 cm and 1.6 ± 0.3 cm for full-FOV images corrected with RPG and topup and 0.6 ± 0.2 cm and 0.7 ± 0.2 for reduced-FOV images (Table 4).

Axillary nodes were more frequently observed ($P < 0.05$) in 168/169 (99%) of the cases in full-FOV EPI images, while in reduced-FOV images, full evaluation of the nodes was attainable in 69% of the cases (reader 1 answered Yes in 117 cases; reader 2, in 118 cases), partially attainable in 21% of the cases (reader 1, answered Partially in 33 cases; reader 2, in 38 cases), and unattainable in 9% of the cases (reader 1 answered No in 19 cases; reader 2, in 13 cases). In a total of 52 cases (31%), evaluation of axillary nodes was determined partial or unattainable. To investigate this further, the distance between the most anterior section of the breast and the edge of the FOV was measured. In 29/52 (or 29/169, 17%) cases, the FOV could have been placed further anteriorly between 0.5 cm and 2.7 cm to increase axillary coverage while allowing for 1 cm between breast tissue and FOV edge. No significant inter-reader difference was detected, and Cohen's Kappa was above 95%, as proof of high concordance, for each stratification.

Residual distortion artifacts in the nipple region were more frequently observed ($P < 0.05$) in full-FOV than in reduced-FOV images. In 157/169 (93%) of the cases, RPG was unable to correct these artifacts in full-FOV EPI data (Figure 3, green arrows). In the remaining 12/169 (7%) of the cases in which the distortion artifact in the nipple area was accurately corrected by RPG, the breast shape was round and the initial distortion was not pronounced (similar to reduced-FOV EPI images). This artifact was not observed in any of the reduced-FOV EPI data sets.

Discussion

In the present study, we evaluated the performance of a prospective distortion reduction method used in conventional EPI and in combination with a custom version of RPG and FSL topup. Furthermore, a reader study was performed to evaluate differences in axillary coverage and residual artifacts between full- and reduced-FOV images.

Other advanced MRI methods have been implemented to minimize distortion artifacts in breast EPI data. For instance, Taviani et al incorporated parallel imaging and reduced-FOV DW-MRI to successfully produce high-resolution images ($0.8 \times 0.8 \times 4.0$ mm^3) with minimal distortion artifacts.[11] Similarly, Lee et al developed a strategy in which B_0-mapping was performed prospectively during prescan, adding ∼2 minutes of scan time. B_0 inhomogeneities were then minimized by dynamically updating per-slice shimming through the EPI acquisition, resulting in reduced distortion artifacts.[22,23] The performance of several prospective and retrospective distortion correction strategies for breast DW-EPI were compared by Hancu et al.[22] Similar to the results of the present study, findings by Hancu et al suggested that a combination of prospective and retrospective strategies (in their case, acquisition with dynamic per-slice shimming[23] and postprocessing with RPG[17]) may be necessary to produce breast EPI data with minimal geometric distortion.[22]

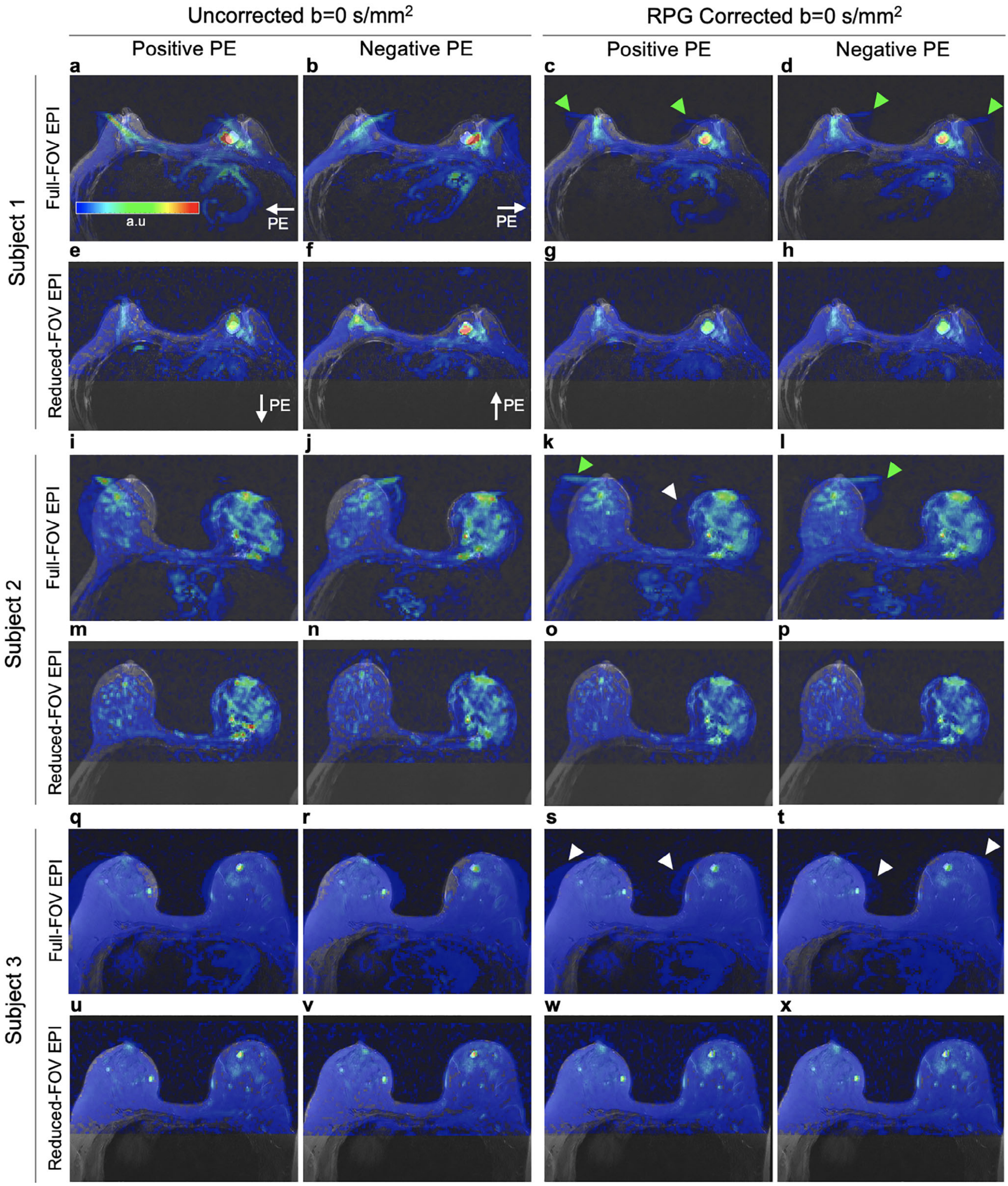

FIGURE 3: Overlay of uncorrected and reversed polarity gradient (RPG) corrected full- and reduced-FOV EPI data on anatomical RARE images in three participants. Data were acquired in the positive (first column) and negative (second column) PE trajectory polarities and were both corrected for geometric distortions using the reversed phase gradient (RPG) retrospective approach (third and fourth columns). Arrows indicate residual distortion in the breast fatty tissue (white) and nipple region (green) after distortion correction with RPG. a.u. = arbitrary units; PE = phase encoding; EPI = echo-planar imaging; FOV = field of view; RARE = rapid acquisition with relaxation enhancement.

The performance of RPG in correcting the geometric distortion from full-FOV DW-MRI breast data (acquired with parallel imaging) was previously evaluated by Teruel et al.[19] Results showed improved spatial agreement between DW and anatomical images.[19] However, the work by Teruel et al was performed with images collected on a

TABLE 4. Mean, Median, 95th Percentile, and Maximum Displacements Between Uncorrected and Corrected Low b-value Volumes

FOV EPI Data	Correction Method	Mean Displacement (cm)	Median Displacement (cm)	Mode Displacement (cm)	95th Percentile Displacement (cm)	Maximum Displacement (cm)
Full-FOV	RPG	0.4 ± 0.1	0.4 ± 0.1	0.3 ± 0.3	1.2 ± 0.3	2.5 ± 0.9
	Topup	0.6 ± 0.1	0.5 ± 0.1	0.4 ± 0.3	1.6 ± 0.3	4.8 ± 1.8
Reduced-FOV	RPG	0.2 ± 0.1	0.2 ± 0.1	0.1 ± 0.1	0.6 ± 0.2	1.5 ± 1.4
	Topup	0.3 ± 0.1	0.2 ± 0.1	0.1 ± 0.2	0.7 ± 0.2	2.1 ± 0.7

Data were estimated within the reduced field of view (FOV) for both echo-planar imaging (EPI) data sets corrected for distortion artifacts with both reversed polarity gradient (RPG) and topup.

single breast in the sagittal plane, which is not representative of typical clinical breast imaging. In contrast, the data in the present study were acquired in the axial plane, which is the standard in clinical breast MRI protocols, offering a more translational evaluation of RPG performance. Of note, parallel imaging was not used in the present study due to technical limitations. Specifically, it was only possible to simultaneously select two of the following methods at a time: back-to-back positive and negative PE data collection, reduced-FOV EPI, and parallel imaging. In the future, we expect to integrate all three methods and both reduce the initial magnitude of distortion artifacts and increase the spatial resolution of DW-MRI.

The implementation of RPG used in this study differed from that originally described by Holland et al[17] in which input volumes were resampled to an isotropic resolution and proton normalization was not applied. The performances of RPG and topup were similar as evaluated by residual distortions and reduction in CV of ADC values. However, while topup performed better in correcting the distortion artifact in the medial region, it incorporated spurious signal intensity variations in homogeneous regions of the breast phantom (Figure 1e, dotted region) not present in RPG. This phenomenon was previously observed by the authors in RPG-corrected images when subtle motion was present between uncorrected positive and negative PE volumes for brain applications. The current version of RPG does not perform the final proton density normalization (normalization by the Jacobian of the resulting displacement field) to avoid incorporating spurious signal intensity variations that may be mistakenly attributed to pathological processes. Proton normalization in FSL's topup implementation may be a reason why it outperforms RPG in correcting the distortion in the medial region, at the risk of incorporating spurious signal intensities to the corrected images. Overall, both techniques improve distortion correction, and based on this evaluation, both will improve the utility of breast diffusion data compared with the standard practice which does not include distortion correction.

Full- and reduced-FOV EPI data were collected with identical pulse sequence parameters, except for the PE direction. Hence, distortion artifacts were of different magnitude and prominent along different axes. A relevant and common example of this occurs in the nipple and medial regions of breasts, where the distortion artifact is, in most cases, uncorrectable with RPG on full-FOV EPI data. Although the comparison is imperfect due to the difference in the PE direction, nipple and medial regions' distortions were decreased and then corrected with RPG on reduced-FOV EPI data. The reduced-FOV EPI methods produce images with decreased distortion artifact magnitude. The estimated magnitude of the distortion correction was in good agreement with the expected distortion reduction between both methods as the PE direction FOV reduction factor was 2. However, chemical shifts between water and fat in both frequency and PE directions are not addressed by RPG. Reduced-FOV EPI images exhibit decreased signal-to-noise ratios compared to conventional EPI, as only a fraction of k-space data is collected. This was also reflected in the higher MI between full-FOV EPI and RARE images, compared to that between reduced-FOV EPI and RARE images. Further studies evaluating the diagnostic value of reduced-FOV EPI remain to be performed.

Limitations

The fact that full- and reduced-FOV EPI data were collected in opposite PE directions complicates the comparison between the magnitude and characteristics of original and residual distortion artifacts. Nonetheless, the results of breast phantom experiments show that the magnitude of original and residual distortions is significantly smaller in reduced-FOV images, while in in vivo data, the magnitude of the distortion was largest at the nipple region even after distortion correction.

Diffusion MRI is not currently specific to discriminating between healthy and metastatic nodes, as normal lymph nodes demonstrate restricted signal similar to malignant nodes.[24,25] Morphology and size of nodes are still the characteristics to suggest metastatic nodes. Thus, the importance of accurate evaluation of breast tissue and primary breast lesions is the current focus of breast diffusion MRI, rather than the axilla where diffusion in general is limited in adding value above basic anatomic imaging. However, in the present study, good visualization of the axilla was attained in 118/169 (70%) cases, and in 29/52 cases, axilla coverage could have been improved by adjustment of the FOV prescription. In large patients, the use of reduced FOV may be problematic, and an alternative may be to reduce the PE direction FOV by a smaller factor. In that case, images will become more severely affected by cardiac and breathing motion artifacts and the use of full-FOV EPI with parallel imaging may be advantageous.

A technical challenge limiting the use of DW-MRI as a screening tool is the limited spatial resolution that prevents the visualization of small lesions without using high-resolution CE-MRI. Recent technical developments have contributed to increased breast DW-MRI resolution and simultaneous reduction of the distortion artifacts affecting single-shot EPI.[11,26,27] However, distortion artifacts are still present in high-resolution DW images,[26] suggesting that further improvement in distortion correction may be attained by incorporating the use of RPG.

Conclusions

Our study demonstrated that RPG decreased distortions due to B_0 inhomogeneity in breast MRI. Based on the present work, breast EPI data with reduced distortion artifact can be readily achieved by combining prospective and retrospective correction strategies such as reduced-FOV EPI and RPG. Finally, we established the utility of reduced-FOV in reducing the magnitude of distortion artifacts.

Acknowledgments

This work was supported by the GE Healthcare, RSNA Research Resident Grant, and California Breast Cancer Research Program Early Career Award

References

1. Cancer Facts & Figures 2019. Atlanta, GA, USA. 2019. p. 1–76.
2. SEER Cancer Statistics Review Based on November 2018 SEER data submission, posted to the SEER web site, April 2019. 1975-2016. https://seer.cancer.gov/csr/1975_2016/
3. Mainiero MB, Moy L, Baron P, et al. ACR appropriateness criteria(®) breast cancer screening. J Am Coll Radiol 2017;14(11s):S383-s90.
4. Orel SG, Schnall MD. MR imaging of the breast for the detection, diagnosis, and staging of breast cancer. Radiology 2001;220(1):13-30.
5. Sentís M. Imaging diagnosis of young women with breast cancer. Breast Cancer Res Treat 2010;123(Suppl 1):11-13.
6. Zhang L, Tang M, Min Z, Lu J, Lei X, Zhang X. Accuracy of combined dynamic contrast-enhanced magnetic resonance imaging and diffusion-weighted imaging for breast cancer detection: A meta-analysis. Acta Radiologica (Stockholm, Sweden: 1987) 2016;57(6):651-660.
7. Kanda T, Ishii K, Kawaguchi H, Kitajima K, Takenaka D. High signal intensity in the dentate nucleus and globus pallidus on unenhanced T1-weighted MR images: Relationship with increasing cumulative dose of a gadolinium-based contrast material. Radiology 2014;270(3):834-841.
8. Partridge SC, McDonald ES. Diffusion weighted magnetic resonance imaging of the breast: Protocol optimization, interpretation, and clinical applications. Magn Reson Imaging Clin N Am 2013;21(3):601-624.
9. Thoeny HC, Ross BD. Predicting and monitoring cancer treatment response with diffusion-weighted MRI. J Magn Reson Imaging 2010;32(1):2-16.
10. Brown R, Cheng Y, Haacke M, Thompson M, Venkatesan R. Magnetic resonance imaging: Physical principles and sequence design. In: Brown R, Cheng Y, Haacke M, Thompson M, Venkatesan R, editors. *Magnetic resonance imaging*. 2nd ed.: Chichester, UK: John Wiley & Sons, Inc; 2014. p i-xxxii.
11. Taviani V, Alley MT, Banerjee S, et al. High-resolution diffusion-weighted imaging of the breast with multiband 2D radiofrequency pulses and a generalized parallel imaging reconstruction. Magn Reson Med 2017;77(1):209-220.
12. Saritas EU, Cunningham CH, Lee JH, Han ET, Nishimura DG. DWI of the spinal cord with reduced FOV single-shot EPI. Magn Reson Med 2008;60(2):468-473.
13. Thierfelder KM, Scherr MK, Notohamiprodjo M, et al. Diffusion-weighted MRI of the prostate: Advantages of zoomed EPI with parallel-transmit-accelerated 2D-selective excitation imaging. Eur Radiol 2014;24(12):3233-3241.
14. Thierfelder KM, Sommer WH, Dietrich O, et al. Parallel-transmit-accelerated spatially-selective excitation MRI for reduced-FOV diffusion-weighted-imaging of the pancreas. Eur J Radiol 2014;83(10):1709-1714.
15. Jin N, Deng J, Zhang L, et al. Targeted single-shot methods for diffusion-weighted imaging in the kidneys. J Magn Reson Imag 2011;33(6):1517-1525.
16. Jezzard P, Balaban RS. Correction for geometric distortion in echo planar images from B0 field variations. Magn Reson Med 1995;34(1):65-73.
17. Holland D, Kuperman JM, Dale AM. Efficient correction of inhomogeneous static magnetic field-induced distortion in Echo planar imaging. Neuroimage 2010;50(1):175-183.
18. Rakow-Penner RA, White NS, Margolis DJA, et al. Prostate diffusion imaging with distortion correction. Magn Reson Imaging 2015;33(9):1178-1181.
19. Teruel JR, Fjøsne HE, Østlie A, et al. Inhomogeneous static magnetic field-induced distortion correction applied to diffusion weighted MRI of the breast at 3T. Magn Reson Med 2015;74(4):1138-1144.
20. Keenan KE, Wilmes LJ, Aliu SO, et al. Design of a breast phantom for quantitative MRI. J Magn Reson Imag 2016;44(3):610-619.
21. Cover T, Thomas J. *Elements of information theory*. 2nd ed. Hoboken, NJ, USA; Wiley Interscience; 2006.
22. Hancu I, Lee SK, Hulsey K, et al. Distortion correction in diffusion-weighted imaging of the breast: Performance assessment of prospective, retrospective, and combined (prospective + retrospective) approaches. Magn Reson Med 2017;78(1):247-253.
23. Lee SK, Tan ET, Govenkar A, Hancu I. Dynamic slice-dependent shim and center frequency update in 3 T breast diffusion weighted imaging. Magn Reson Med 2014;71(5):1813-1818.
24. Fornasa F, Nesoti MV, Bovo C, Bonavina MG. Diffusion-weighted magnetic resonance imaging in the characterization of axillary lymph nodes in patients with breast cancer. J Magn Reson Imag 2012;36(4):858-864.

25. Rautiainen S, Könönen M, Sironen R, et al. Preoperative axillary staging with 3.0-T breast MRI: Clinical value of diffusion imaging and apparent diffusion coefficient. PLoS One 2015;10(3): e0122516.

26. Naranjo ID, Gullo RL, Morris EA, et al. High-spatial-resolution multishot multiplexed sensitivity-encoding diffusion-weighted imaging for improved quality of breast images and differentiation of breast lesions: A feasibility study. Radiology 2020;2(3):e190076.

27. Hu Y, Ikeda DM, Pittman SM, et al. Multishot diffusion-weighted MRI of the breast with multiplexed sensitivity encoding (MUSE) and shot locally low-rank (shot-LLR) reconstructions. J Magn Reson Imaging 2020;53(3):807–817.